MAIN TEXT

Fluctuating environments promote evolvability by shaping adaptive variation accessible to populations

Bhaskar Kumawat[1], Alexander Lalejini[1,2], Monica Acosta[1,2], *Luis Zaman[1,2]

[1] Department of Ecology and Evolutionary Biology, University of Michigan, Ann Arbor, MI, 48109, USA
[2] Center for the Study of Complex Systems, University of Michigan, Ann Arbor, MI, 48109, USA
(* Corresponding author, zamanlh@umich.edu)

SUMMARY

Evolvability is defined as the capacity of populations to generate adaptive variation that promotes evolution by natural selection[1–4]. Lineages in a fluctuating environment must rapidly adapt to different states of the environment to survive. One possible solution is for populations to evolve increased evolvability. However, in individual environmental states, there is no selection pressure on a population to make adaptive variation more accessible. Whether natural selection can drive organisms to become more evolvable is still unclear[5–7]. Here we show that evolution in fluctuating environments can lead to an increase in the mutational accessibility of adaptive variation. We find that genotypes from populations that evolve in environments fluctuating between two states have a larger proportion of mutants adapted to alternate environments when compared to genotypes in a static environment. These genotypes also encode more information about the nature of the fluctuating environments in their mutational neighborhood. Analysis of evolved lineages shows that the lineages survive by continually fixing adaptive mutations, and localizing on areas of the genotype space with increased access to alternate phenotypes. We find that this increase in adaptive mutants is contingent on the rate at which the environment fluctuates. To further understand this phenomenon, we explore evolutionary dynamics in a model with explicit genetic structure in fluctuating environments. Results from this simple model point toward a mechanism by which changing environments promote the localization of populations on edges in genotype space, where a diverse repertoire of variants is available through mutations. Populations then stochastically evolve along these boundaries and end up in highly evolvable locations between alternatively adapted phenotypes. Thus, we demonstrate that evolvability can and does evolve even in simple systems, and likely has been playing an important role in the adaptation of living systems.

Populations depend on adaptive variation to continually evolve and thus increase in fitness by natural selection. However, finite populations are inherently limited in their ability to create genetic variation. *De novo* mutations only arise on the background of existing genotypes in the population, and thus the location and spread of a population in genotype-space vitally determines its long-term success[8–10]. Changing environments pose an additional hurdle for evolving populations, since they demand continuous adaptation to different selection pressures and, thus, a constant supply of adaptive variation[11–18]. An evolving population in such an environment would survive better if mutant genotypes give rise to phenotypes adapted to the different environments potentially encountered throughout evolution[19]. However, whether natural selection can regulate the accessibility of adaptive mutants is still widely debated[1–7,20,21].

The fundamental source of conflict is that the ability to generate adaptive variants fit for some future environment is not directly beneficial to the present population, but rather has benefits for future descendants of extant organisms. The ability to generate adaptive variation for future environments, or *evolvability,* therefore must be a trait selected at a larger scale than the individual organism (e.g., entire lineages or clades)[1,22,23]. Evolution on short time scales, however, is extremely myopic and can only favor traits that are immediately beneficial[6,7]. In fact, it is well known that evolution in static environments favors increased robustness to mutations, a property directly in conflict with adaptive variation to a different, unrealized, environment[24,25]. Despite these objections, a variety of mechanisms that enhance organismal evolvability have been studied. These include increased mutation rates, developmental plasticity, the flexibility of gene interaction networks, recombination, and epigenetic modification[26–29]. However, all these potential mechanisms of evolvability require highly evolved biological machinery which cannot be disentangled from natural selection on their associated (i.e., directly beneficial) traits[5]. To empirically address this long-standing issue, we need an evolutionary model system unencumbered by such historical selection. Here, we turn to the Avida[30] digital evolution platform to test if and how the nature of mutational variation accessible to evolving populations itself evolves when the environment fluctuates between alternative states.

We found that evolvability is indeed evolvable, and is driven by populations localizing in atypical regions of genotype space. These regions were dramatically enriched in adaptive mutations, where small genetic changes (i.e., point mutations) had large phenotypic effects. We additionally found that the mutational neighborhood of evolved genotypes encoded measurable information about the nature of environments experienced during evolution. Changing environments consistently favored rare adaptive fixations on lineages, but only if the environments changed with intermediate frequency. Over long timescales, populations evolved a steady increase in available adaptive variation, ending up with a trade-off between adaptations to alternative environments. These results led us to propose a process whereby populations localize on boundaries between alternatively favorable phenotypes, and we further demonstrated these dynamics using a simple genetically explicit Wright-Fisher simulation.

Accessibility of alternative phenotypes

In Avida, organisms are autonomous, self-replicating computer programs that compete for space and processing time in a virtual world (Fig 1a). These organisms possess a *genome* - a linear sequence of computer instructions - that is executed during an organism's lifetime. The genome encodes a simple replication loop, where instructions are copied from one location in memory to another, and additional computational routines (Fig 1b). The copying of instructions during reproduction is prone to errors and gives rise to mutations in the offspring's genome (Fig 1c, red circles).

We classify the computations performed by organisms into six different tasks. These tasks, if performed during an organism's lifetime, award the organism with a fitness multiplier, which in turn modifies its rate of execution and reproduction. For the experiments presented here, we use a mapping between tasks and their rewards such that organisms gain an incremental fitness benefit for each task performed within complementary sets of tasks in two alternate environments, ***A*** and ***B*** (Fig 1b, right). The tasks in the alternate set in each environment are assigned a fractional fitness multiplier and thus decrease organism fitness when executed. Henceforth, we use *cognate* to denote pairs of tasks that are rewarded or penalized together within an environment. Each replicate starts with a single ancestral organism in the Avida world and the environments are varied in different ways to create four environmental change *regimes* - *Const-A*, *Const-B*, *Cyclic*, and *Random* (Fig 2a). Each regime ends with approximately 30 generations of evolution in a static

terminal environment. The overall duration of an evolutionary run is approximately 30,000 generations (see Methods).

To test for the accessibility of phenotype-altering mutations, we isolated the most frequent genotype (the *dominant* genotype) from each evolved replicate population and created all possible single and double point mutations. We measured the phenotypes encoded by these mutants and counted the number of mutants perfectly adapted - and complementary to - the terminal environment. We found that dominant genotypes from populations that evolved under the *Cyclic* regime had a significantly greater number of mutants adapted to the alternate environment (Fig 2b, right). The difference between *Const-A* and *Cyclic* was striking, with around 1000 times more mutants that were perfectly adapted to the environment complementary to the terminal one. The stereotypical nature of environmental change also aided this increase; rewarding a completely random set of tasks did increase the number of alternate adapted mutants but to a much lesser extent (*Random* regime). The overall distribution of mutants with different adaptations is shown in Extended Data Figure 1a. Surprisingly, this increase in the number of mutants adapted to the alternate environment was not at the cost of mutants adapted to the terminal environments (i.e., robustness; Extended Data Figure 1b).

Information encoded in the mutational neighborhood

Adaptation, by definition, leads to organisms that are more capable of surviving and thriving in their environments (i.e., are more "fit"). As populations evolve greater fitness, information about the environment also accumulates in the organisms' genomes. For example, if an organism contains genes used for blubber development, we can be fairly certain that it is an aquatic mammal[31]. We have already shown that evolution in cyclically changing environments induced an increase in the number of mutants adapted to the alternate environment. Since the alternative environments we used were complementary, we hypothesized that additional information about the way environments fluctuated would end up encoded in evolved digital genomes.

To test this, we checked if certain task pairs were overrepresented in the set of mutants of the dominant genotypes. Specifically, we calculated the normalized pointwise mutual information (NPMI) using the joint probability of picking a mutant that could perform both tasks in a pair, and the marginal probability of picking mutants that could perform the individual tasks (See Methods). Mutants of organisms from constant environments exhibited positive correlations for cognates, and negative correlations for non-cognate tasks (Figure 3a, top-left and top-right). This is expected given the general observation that mutants of a genotype are likely to express similar phenotypes[24,32–36].

Surprisingly, we found that evolution in the *Cyclic* regime amplified both the positive NPMI between cognate and the negative NPMI between non-cognate tasks (Figures 3a and 3b). This implied that cognate pairs were over-represented in the neighborhood of dominant genotypes evolved in cyclic environments and that non-cognate pairs of tasks were underrepresented. Hence, not only were the organisms easily able to create mutants adapted to alternate environments, but it also became more challenging to generate mismatched phenotypes. In other words, evolution led to a genetic architecture that encoded more precise information about the structure of the changing environments. Interestingly, we did not find a significant increase in NPMI in the *Cyclic* regime when the average environment switching time was increased or decreased by an order of magnitude (Extended data Fig 2a,b). This decay in NPMI at different switching rates was correlated with a decrease in the number of mutants adapted to the terminal environments (Extended data Fig 2c).

Adaptation on the lineage

To analyze the dynamics of adaptation over evolutionary time, we obtained the lineages for the dominant genotypes by tracing mutation events back in time, ending with the ancestral genotype (Figure 4a). Then, we measured the phenotypes expressed by each genotype along the lineage and plotted them against the state of the environment at the time the mutation occurred (Figure 4b). We discovered that lineage genotypes early in evolutionary time were adapted only imperfectly to the two environments in the *Cyclic* regime. After 30,000 generations of evolution, the lineages were able to perfectly adapt to both environments, where they switched phenotypes in a way that tracked the environment state (Figure 4b and 4c). Evolution in an environment that switched ten times faster did not admit environment state tracking. Instead, lineages in rapidly changing environments acquired a phenotype imperfectly adapted to both (Figure 4c, bottom and Extended Data Figure 3). Lineages in the constant regimes attained a phenotype perfectly adapted to the environment and did not change their phenotype thereafter (Figure 4c, top and Extended Data Figure 3).

These results suggested that phenotypic adaptation in constant environments was limited to early time points during evolution. To probe this further, we looked for signatures of adaptation along the lineage. Having a record of the complete lineage history and the ability to characterize genotypes' mutational neighborhoods, we calculated the likelihood of realized phenotypic change along the lineage. This likelihood was calculated by measuring the fraction of single mutants with the next realized phenotype in the current genotype's mutational neighborhood. The negative logarithm of the likelihood gives the rarity of the realized change evaluated for each mutational event. Large positive deviations in the negative log-likelihood indicate mutation events where a phenotype with a very low frequency in the immediate mutational neighborhood of the lineage genotype was subsequently "fixed", an event that is likely only if selection for that phenotype was driving its dominance. As expected, we observed these signatures of adaptation (as peaks in the rarity curves) only early in evolution under the constant regimes (Figure 4d, top). However, in the *Cyclic* regime, lineages consistently fixed mutationally rare phenotypes over the course of evolution (Figure 4d, bottom). These continuous signatures of adaptation disappeared completely if the environments changed extremely rapidly and became less frequent with slower environment switching rates (Extended Data Figure 4).

Accessibility of adaptive variation over evolutionary time

To survey the mutational accessibility of adaptive variation over the course of evolution, we generated all single mutants for genotypes along the dominant lineage from each replicate population (Figure 4a). Then, we measured their phenotypes and counted the number of mutants adapted to both the alternate and the contemporaneous environmental states present when the genotypes appeared in the lineage. In line with our previous observations, we found that genomes late in evolutionary time had a much greater number of mutants adapted to their alternate environment (Figure 5a). We did find a few genotypes along the lineage that failed to track the environment (Figure 4b, mismatched points). For subsequent analysis, we removed these environment-mismatched genotypes and measured the number of mutants of the remaining lineage genotypes adapted to the alternate environments. We found that the mutational neighborhood of lineages evolving in the *Cyclic* regime accumulated more mutants adapted to the alternate environment over time (Figure 5b).

To characterize how each lineage moved through genetic space, we measured how the distribution of perfectly adapted single mutants (to either environment) changed after each fixed mutational step along the lineage (Figure 5c, top). Based on our results thus far, we hypothesized that the lineages move from genetic regions dominated by intermediate-adapted phenotypes to regions that lie on the boundary between perfectly adapted phenotypes. This hypothetical process would lead to lineages approaching a 1:1 tradeoff between changes in the number of mutants with perfectly adapted phenotypes as the populations localize on highly evolvable boundaries (Figure 5c, bottom). Comparing the changes in mutant phenotypes at early, middle, and late evolutionary time points did indeed reveal a 1:1 tradeoff in the *Cyclic* regime (Figure

5d). The constant environments did not show a similar pattern of increased tradeoffs (Extended Data Figure 5). Interestingly, we saw zero mutation events with correlated increases where mutants had adapted to both environments, indicating that lineages never moved directly from an intermediate-adapted region to an evolvable region of the genotype space (Extended Data Figure 5).

Localization on the genotype space

To test the validity of this hypothetical model in a more transparent system, we simulated evolution using an explicit two-dimensional genotype-phenotype map (Extended Data Figure 6a). Each genotype (pixel) in this map had four mutants (the four adjacent pixels in the genotype's Von Neumann neighborhood). A genotype belonged to one of three phenotypes - *Intermediate (I)*, *A-adapted (A)*, and *B-adapted (B)*. Genotypes belonging to the intermediate phenotype had a fitness of 1.0 in all environments. On the other hand, phenotypes *A* and *B* fluctuated between a relative fitness of 0.8 and 2.0 depending on the environment state (Extended Data Figure 6a). For these experiments, we switched the environment state every 100 generations on average (Poisson rate parameter of 10^{-2}, see Methods). To simulate selection, genotypes were sampled using Wright-Fisher dynamics where 1% of the selected offspring genotypes were mutated. The number of mutations was sampled from a Poisson distribution (see Methods). We evolved 20 replicate populations on this genotype-phenotype map for 75 million generations. Initial populations all started out in the leftmost part of the intermediate phenotype region.

Over the course of evolution, we saw that populations on the genotype-phenotype map first localized on the *I-A and I-B* boundaries, and then searched the region stochastically until they localized on a region where easy mutation to the alternate phenotypes was possible, i.e. the *A-B* boundary (Figures 5e, 5f, and Supplementary Video 1). No such localization was observed under constant environments (Extended Data Figure 6b and Supplementary Video 2). The localization also disappeared at extreme environment switching rates (Extended Data Figure 6b and Supplementary Videos 3 and 4).

Discussion

In this work, we have shown that simple evolutionary dynamics in finite populations are sufficient to drive an increase in evolvability. Specifically, we show that populations evolving in changing environments show consistent signatures of adaptation, have a larger number of mutants adapted to alternate environments, and encode more information about the structure of environments in their mutational neighborhoods when compared to evolution in static environments. Using a simple model of evolution on a 2D genotype space, we demonstrated how selection in alternating environments leads to populations localizing along borders separating phenotypes. Over evolutionary time, populations stochastically explore these *edges* in phenotype space, and eventually localize on highly evolvable boundaries between perfectly adapted phenotypes. This simple process of evolutionary dynamics along phenotypic boundaries can account for many of the complex patterns we observed in our digital evolution experiments, including their sensitivity to the rate of environmental switching.

There is some evidence that environmental change can drive diversification and increased speciation in clades[37–39]. It is known that a changing environment can also allow populations to escape local maxima on the fitness landscape and find novel variation[11,13–15,17,18,40–42]. Our work adds to this knowledge by demonstrating the process by which environmental fluctuations move populations to areas of the genotype space where adaptive variation is easily accessible. The results also point toward the existence of an ideal range of fluctuation rates where environmental change can drive this localization. Future work should seek to develop theory resolving the evolutionary dynamics underlying this phenomenon, specifically the dependence of localization on fluctuation rate and other demographic parameters.

These findings have broad implications in fields that either rely on fluctuating selection as a tool or are sensitive to its consequences. A fluctuating drug regimen is often cited as a solution to the problem of multi-drug resistance in pathogenic bacteria[43–46]. Pinpointing the ideal fluctuation rates for natural bacterial populations will help identify and avoid situations where such a treatment might lead to the evolution of super-evolvable strains. In phage therapy, on the contrary, training phages to infect and lyse bacteria by evolving them under ideal switching rates can lead to more effective *super*-phages that can be trained quickly to treat multiple infections[47]. Environmental change threatens ecological communities at multiple scales and natural selection can sometimes rescue populations facing a high risk of extinction[48]. By identifying species far away from phenotypic boundaries, we might be able to prioritize conservation efforts towards less evolvable populations. In artificial intelligence and evolutionary computing, evolving programs in an environment that rewards different tasks at appropriate time scales might allow tuning of the underlying representation for easier problem-solving[49].

Together, our results demonstrate that evolvability is evolvable even in elementary evolving systems that lack complex biological machinery typically invoked to explain evolvability. This process can be effectively studied using simple models of population dynamics in structured genotype spaces. We thus present a fundamental way that evolution towards phenotypic boundaries in the genotype space can effectively favor evolvability. Our results, which demonstrate an effective process favoring evolvability, offer a partial resolution to an integral part of the call for an extended evolutionary synthesis (EES)[5–7,50].

References

1. Kirschner, M. & Gerhart, J. Evolvability. *Proc. Natl. Acad. Sci.* **95**, 8420–8427 (1998).
2. Payne, J. L. & Wagner, A. The causes of evolvability and their evolution. *Nat. Rev. Genet.* **20**, 24–38 (2019).
3. Wagner, G. P. & Altenberg, L. Perspective: Complex Adaptations and the Evolution of Evolvability. *Evolution* **50**, 967–976 (1996).
4. Riederer, J. M., Tiso, S., van Eldijk, T. J. B. & Weissing, F. J. Capturing the facets of evolvability in a mechanistic framework. *Trends Ecol. Evol.* **37**, 430–439 (2022).
5. Pigliucci, M. Is evolvability evolvable? *Nat. Rev. Genet.* **9**, 75–82 (2008).
6. Lynch, M. The frailty of adaptive hypotheses for the origins of organismal complexity. *Proc. Natl. Acad. Sci.* **104**, 8597–8604 (2007).
7. Sniegowski, P. D. & Murphy, H. A. Evolvability. *Curr. Biol.* **16**, R831–R834 (2006).
8. Yubero, P., Manrubia, S. & Aguirre, J. The space of genotypes is a network of networks: implications for evolutionary and extinction dynamics. *Sci. Rep.* **7**, 13813 (2017).
9. McLeish, T. C. B. Are there ergodic limits to evolution? Ergodic exploration of genome space and convergence. *Interface Focus* **5**, 20150041 (2015).
10. Aguirre, J., Catalán, P., Cuesta, J. A. & Manrubia, S. On the networked architecture of genotype spaces and its critical effects on molecular evolution. *Open Biol.* **8**, 180069 (2018).
11. de Vos, M. G. J., Dawid, A., Sunderlikova, V. & Tans, S. J. Breaking evolutionary constraint with a tradeoff ratchet. *Proc. Natl. Acad. Sci.* **112**, 14906–14911 (2015).
12. Matuszewski, S., Hermisson, J. & Kopp, M. Catch Me if You Can: Adaptation from Standing Genetic Variation to a Moving Phenotypic Optimum. *Genetics* **200**, 1255–1274 (2015).
13. Steinberg, B. & Marc Ostermeier. Environmental changes bridge evolutionary valleys. *Sci. Adv.* **2**, e1500921 (2016).
14. Xue, B., Sartori, P. & Leibler, S. Environment-to-phenotype mapping and adaptation strategies in varying environments. *Proc. Natl. Acad. Sci.* **116**, 13847–13855 (2019).
15. Maltas, J., McNally, D. M. & Wood, K. B. Evolution in alternating

environments with tunable interlandscape correlations. *Evolution* **75**, 10–24 (2021).

16. King, J. G. & Hadfield, J. D. The evolution of phenotypic plasticity when environments fluctuate in time and space. *Evol. Lett.* **3**, 15–27 (2019).
17. Botero, C. A., Weissing, F. J., Wright, J. & Rubenstein, D. R. Evolutionary tipping points in the capacity to adapt to environmental change. *Proc. Natl. Acad. Sci.* **112**, 184–189 (2015).
18. Boyer, S., Hérissant, L. & Sherlock, G. Adaptation is influenced by the complexity of environmental change during evolution in a dynamic environment. *PLOS Genet.* **17**, e1009314 (2021).
19. Meyers, L. A. & Bull, J. J. Fighting change with change: adaptive variation in an uncertain world. *Trends Ecol. Evol.* **17**, 551–557 (2002).
20. Díaz Arenas, C. & Cooper, T. F. Mechanisms and selection of evolvability: experimental evidence. *FEMS Microbiol. Rev.* **37**, 572–582 (2013).
21. Tikhonov, M., Kachru, S. & Fisher, D. S. A model for the interplay between plastic tradeoffs and evolution in changing environments. *Proc. Natl. Acad. Sci.* **117**, 8934–8940 (2020).
22. Doolittle, W. F. Making the Most of Clade Selection. *Philos. Sci.* **84**, 275–295 (2017).
23. Okasha, S. Multilevel Selection and the Major Transitions in Evolution. *Philos. Sci.* **72**, 1013–1025 (2005).
24. van Nimwegen, E., Crutchfield, J. P. & Huynen, M. Neutral evolution of mutational robustness. *Proc. Natl. Acad. Sci.* **96**, 9716–9720 (1999).
25. Wilke, C. O., Wang, J. L., Ofria, C., Lenski, R. E. & Adami, C. Evolution of digital organisms at high mutation rates leads to survival of the flattest. *Nature* **412**, 331–333 (2001).
26. Bedau, M. A. & Packard, N. H. Evolution of evolvability via adaptation of mutation rates. *Biosystems* **69**, 143–162 (2003).
27. Parter, M., Kashtan, N. & Alon, U. Facilitated Variation: How Evolution Learns from Past Environments To Generalize to New Environments. *PLOS Comput. Biol.* **4**, e1000206 (2008).
28. Crombach, A. & Hogeweg, P. Evolution of Evolvability in Gene Regulatory Networks. *PLOS Comput. Biol.* **4**, e1000112 (2008).
29. Skanata, A. & Kussell, E. Evolutionary Phase Transitions in Random Environments. *Phys. Rev. Lett.* **117**, 038104 (2016).
30. Ofria, C. & Wilke, C. O. Avida: a software platform for research in computational evolutionary biology. *Artif. Life* **10**, 191–229 (2004).
31. Yuan, Y. *et al.* Comparative genomics provides insights into the aquatic adaptations of mammals. *Proc. Natl. Acad. Sci.* **118**, e2106080118 (2021).
32. Payne, J. L. & Wagner, A. The Robustness and Evolvability of Transcription Factor Binding Sites. *Science* **343**, 875–877 (2014).
33. Wagner, A. Robustness and evolvability in living systems. in *Robustness and evolvability in living systems* (Princeton university press, 2013).
34. Kitano, H. Biological robustness. *Nat. Rev. Genet.* **5**, 826–837 (2004).
35. Greenbury, S. F., Schaper, S., Ahnert, S. E. & Louis, A. A. Genetic Correlations Greatly Increase Mutational Robustness and Can Both Reduce and Enhance Evolvability. *PLOS Comput. Biol.* **12**, e1004773 (2016).
36. Zheng, J., Guo, N. & Wagner, A. Selection enhances protein evolvability by increasing mutational robustness and foldability. *Science* **370**, eabb5962 (2020).
37. Aguilée, R., Gascuel, F., Lambert, A. & Ferriere, R. Clade diversification dynamics and the biotic and abiotic controls of speciation and extinction rates. *Nat. Commun.* **9**, 3013 (2018).
38. Aguilée, R., Claessen, D. & Lambert, A. Adaptive Radiation Driven by the Interplay of Eco-Evolutionary and Landscape Dynamics. *Evolution* **67**, 1291–1306 (2013).
39. Doebeli, M. & Dieckmann, U. Speciation along environmental gradients. *Nature* **421**, 259–264 (2003).
40. Canino-Koning, R., Wiser, M. J. & Ofria, C. Fluctuating environments select for short-term phenotypic variation leading to long-term exploration. *PLOS Comput. Biol.* **15**, e1006445 (2019).
41. Kashtan, N., Noor, E. & Alon, U. Varying environments can speed up evolution. *Proc. Natl. Acad. Sci.* **104**, 13711–13716 (2007).
42. Nahum, J. R. *et al.* Improved adaptation in exogenously and endogenously changing environments. in *Proceedings of the 14th European Conference on Artificial Life ECAL 2017* 306–313 (MIT Press, 2017). doi:10.7551/ecal_a_052.
43. Card, K. J., LaBar, T., Gomez, J. B. & Lenski, R. E. Historical contingency in the evolution of antibiotic resistance after decades of relaxed selection. *PLOS Biol.* **17**, e3000397 (2019).
44. Cisneros-Mayoral, S., Graña-Miraglia, L., Pérez-Morales, D., Peña-Miller, R. & Fuentes-Hernández, A. Evolutionary History and Strength of Selection Determine the Rate of Antibiotic Resistance Adaptation. *Mol. Biol. Evol.* **39**, msac185 (2022).
45. Melnyk, A. H., McCloskey, N., Hinz, A. J., Dettman, J. & Kassen, R. Evolution of Cost-Free Resistance under Fluctuating Drug Selection in Pseudomonas aeruginosa. *mSphere* **2**, e00158-17 (2017).
46. Santos-Lopez, A. *et al.* The roles of history, chance, and natural selection in the evolution of antibiotic resistance. *eLife* **10**, e70676 (2021).
47. Borin, J. M., Avrani, S., Barrick, J. E., Petrie, K. L. & Meyer, J. R. Coevolutionary phage training leads to greater bacterial suppression and delays the evolution of phage resistance. *Proc. Natl. Acad. Sci.* **118**, e2104592118 (2021).
48. Peniston, J. H., Barfield, M., Gonzalez, A. & Holt, R. D. Environmental fluctuations can promote evolutionary rescue in high-extinction-risk scenarios. *Proc. R. Soc. B Biol. Sci.* **287**, 20201144 (2020).
49. Droste, S. & Wiesmann, D. On Representation and Genetic Operators in Evolutionary Algorithms. (1998) doi:10.17877/DE290R-15343.
50. Pigliucci, M. & Muller, G. B. Evolution–the extended synthesis. (2010).

FIGURES

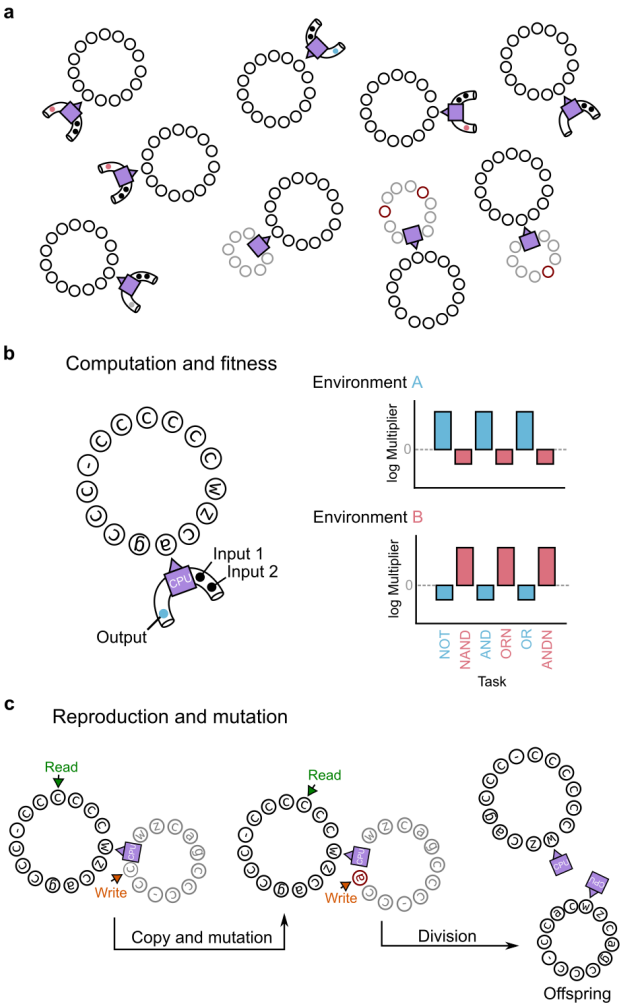

Figure 1: Schematic of digital organisms in Avida. (**a**) An Avida world consists of multiple genomic sequences, encoded as a circular series of instructions (black circles) that can be read by a virtual CPU (purple square) that translates these instructions into organismal function. The main organismal functions include *computation* - where organisms perform logical tasks to increase reproductive efficacy - and *reproduction* - where the sequence instructs the CPU to copy instructions into a new memory location (grey and red circles) (**b**) During computation, the sequence requests inputs from the environment and acts upon these inputs to generate an output (left). We use two environments in this study - A and B - both of which recognize a set of six possible computations or tasks. Successful execution of a task can either increase or decrease the fitness of the organism based on the magnitude of the fitness multiplier in the current environment. In our experiments, environments A and B reward mutually exclusive sets of tasks, while penalizing the alternate set (right; reward multiplier = 2.0; penalty multiplier = 0.8) (**c**) Reproduction occurs when the sequence instructs the CPU to copy itself instruction-by-instruction from a read location (green) to a write location (orange) and subsequently divides (right), producing an offspring with its own CPU. New offspring take over random locations in the Avida world, overwriting any organisms present at those positions. Copying probabilistically induces mutations into the genome (middle, red circle), which act as a source of *de novo* variation for the population.

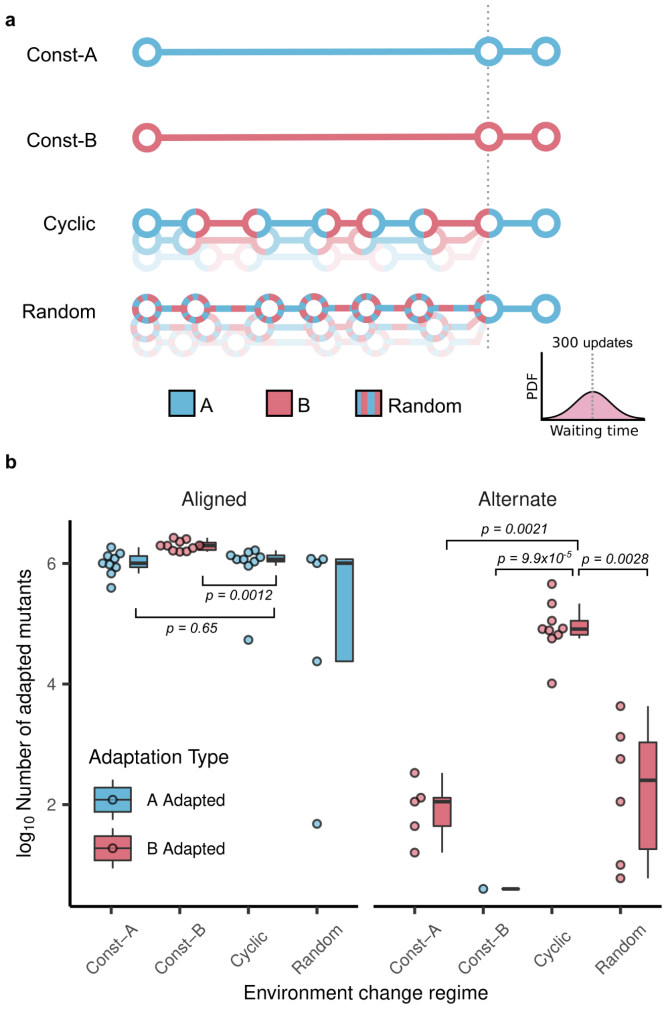

Figure 2: Adaptations in the mutational neighborhood. (**a**) Schematic of the four environment change regimes used in this study. *Const-A* and *Const-B* regimes maintain environments A and B, respectively, over the entire duration of evolution. *Cyclic* switches between the two environments with a waiting time picked from a Gaussian distribution with a mean of 300 updates and an SD of 60 updates. The *Random* regime rewards a randomly picked set of tasks and switches with a similar waiting time distribution as *Cyclic*. Replicate runs for *Cyclic* and *Random* regimes are performed with different samples from the waiting time distributions. All of the regimes end with 300 updates of evolution in a fixed terminal environment (shown after the dotted line). (**b**) The number of point mutants (single and double) of the dominant genotype from the end of the simulation that are either perfectly aligned with the terminal environment (left; Kruskal-Wallis χ^2 = 25.735, df = 3, p-value = 1.084e-05), or perfectly adapted to the alternate environment (right; Kruskal-Wallis χ^2 = 24.155, df = 3, p-value = 2.319e-05) for different environment change regimes. The color of the box plot and accompanying points denotes the adaptation being tested in each case, depending on the terminal environment in a regime (n=10). Note that the y-axis is log-scaled and data points with zero mutants have been removed from the figure. Each point denotes the dominant genotype from one evolved replicate population. The lower and upper edges of the boxes represent the first (Q_1) and third quartiles (Q_3), respectively. The horizontal line through the box indicates the median and the whiskers extend to maximum values within the upper ($Q_3 + 1.5 \times IQR$) and lower fences ($Q_1 - 1.5 \times IQR$), where IQR is the interquartile range ($Q_3 - Q_1$). Pairwise p-values shown in the figure are calculated using a two-tailed Wilcoxon rank-sum test (p-values adjusted using the Benjamini-Hochberg method). Both the Kruskal-Wallis and the Wilcoxon tests were done using non-log-transformed data.

FIGURES

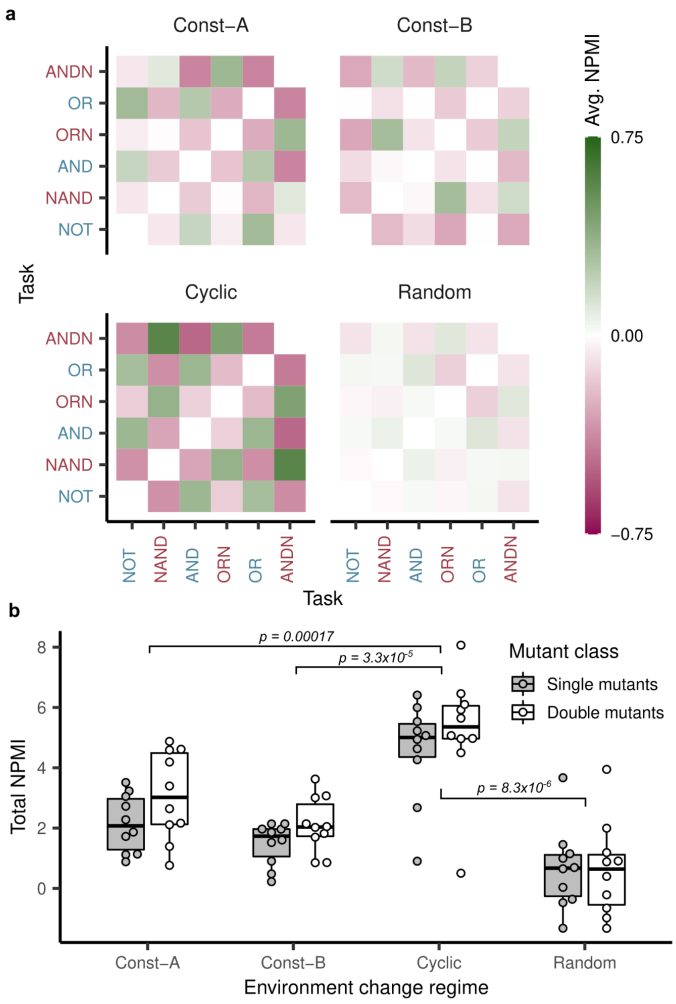

Figure 3: Information in the mutational landscape. (**a**) Heat maps denoting the normalized pointwise mutual information (NPMI; see Methods) values between different task pairs for dominant genotypes isolated from populations evolved in the four regimes. The heat maps are symmetric, and both halves are shown here to aid visualization. The marginal and joint probabilities for different tasks are calculated using only the double mutants of the dominant genotype at the end of the simulation. Labels in blue and red denote tasks rewarded in environments A and B, respectively. Tasks rewarded together in an environment are defined as *cognates*. The NPMI values for each task pair have been averaged across the 10 replicates. (**b**) Total NPMI for the four environment change regimes for both the single and double mutant landscape of evolved genotypes. The total NPMI was calculated by adding up individual NPMI values after assigning them a sign based on the cognate/non-cognate nature of a task pair. Each point denotes the total NPMI calculated using the single or double mutants of the isolated dominant genotypes from 10 different replicate populations. Box plot characteristics are the same as in Figure 2b. NPMI values were found to be significantly different between regimes but not between mutant classes (two-way ANOVA; regime F = 34.178; regime df = 3; regime p-value = 7.59e-14***; class F = 3.120; class df = 1; class p-value = 0.0816). Pairwise p-values shown in the figure are calculated using a two-tailed Wilcoxon rank-sum test (p-values adjusted using the Benjamini-Hochberg method).

FIGURES

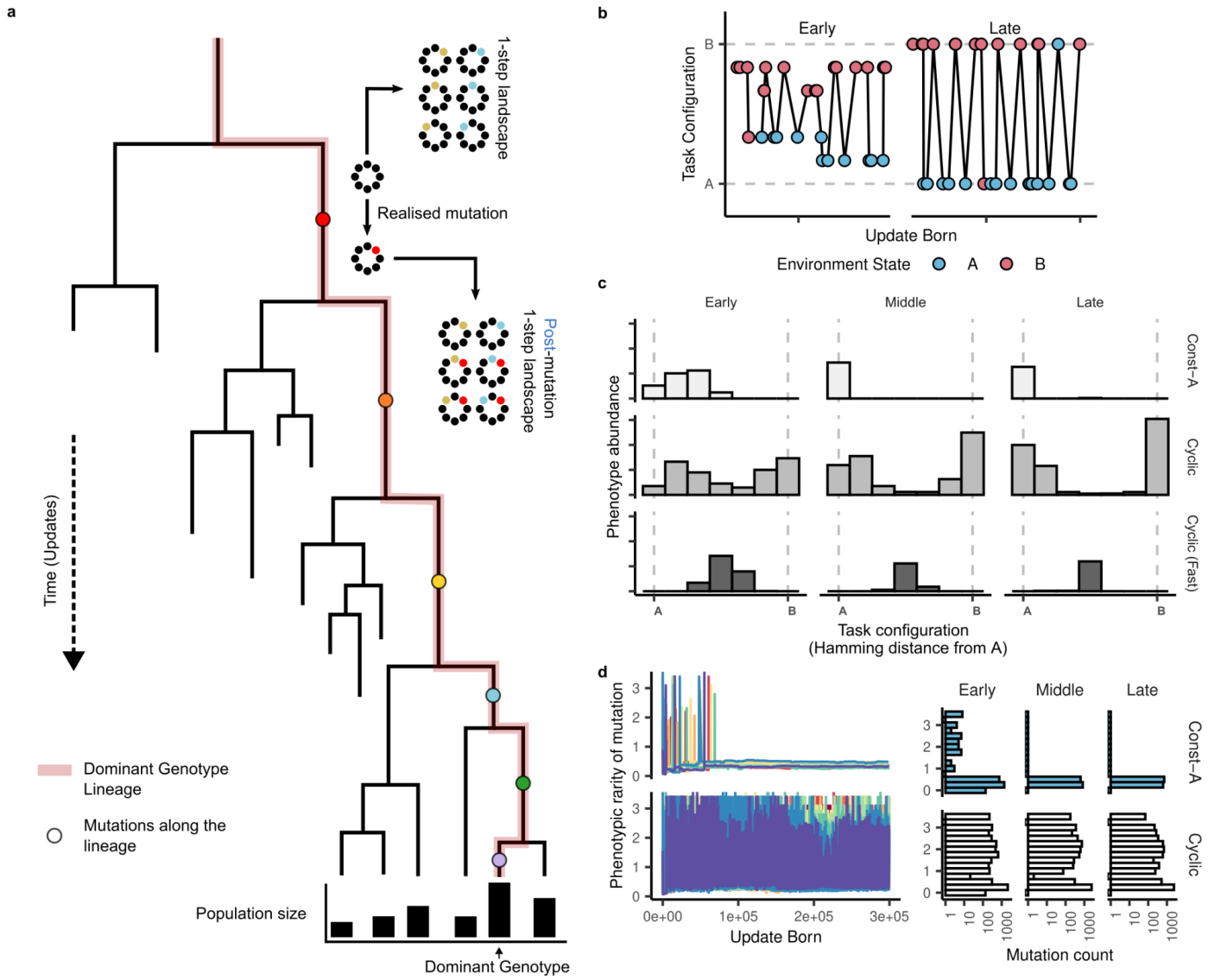

Figure 4: Adaptation along lineages in a changing environment. (**a**) A schematic describing the analysis of progenitor and post-mutation landscapes on the dominant genotype's lineage. The black lines form a phylogeny of sequences (i.e., genotypes) that appear in the Avida world over time. Each node denotes a mutation event, where a new genotype is created through mutation occurring in the progenitor's genotype. The lineage for the dominant genotype is isolated and all point mutants are created, and this is repeated for each sequence along the lineage. We call this set of mutants of a genotype its mutational landscape. The rarity of a phenotypic change can be calculated by determining the fraction of mutants in the progenitor's landscape that have the realized phenotype after mutation. (**b**) Pattern of adaptation on a representative dominant genotype lineage evolving in the *Cyclic* regime. The x-axis denotes the update that a genotype appeared in the lineage through mutation and the y-axis denotes the task configuration of the genotype. Task configuration is calculated as the minimum number of task losses/gains required to be perfectly adapted to environment A, or the Hamming distance of the phenotype from a phenotype perfectly adapted to environment A. Genotypes on the A and B lines on this graph are perfectly adapted to the respective environments. Early and late curves are from updates 10,000-15,000 and 295,000-300,000 respectively. The color of the points denotes the state of the environment at the update the genotype appeared in the lineage. (**c**) Distribution of task configurations for sequences on the dominant genotype lineage evolved under three different environment change regimes (rows) during early, middle, and late evolution (columns). Waiting times in the *Cyclic (fast)* regime are ten times shorter than in the normal *Cyclic* regime. Mutation events along lineages from all ten replicates have been combined in these histograms. (**d**) Rarity of realized phenotypic changes along the lineage during evolution in *Const-A*, and *Cyclic* environments (left). Each curve is a dominant genotype lineage from each of the ten replicates. Histogram of the phenotypic rarity of mutations from early, middle, and late evolution (right). Rarity is measured as the negative log-likelihood of a phenotype change that appears in the lineage (see Methods). The x-axis denotes the number of mutants with a given rarity and has been log-scaled.

FIGURES

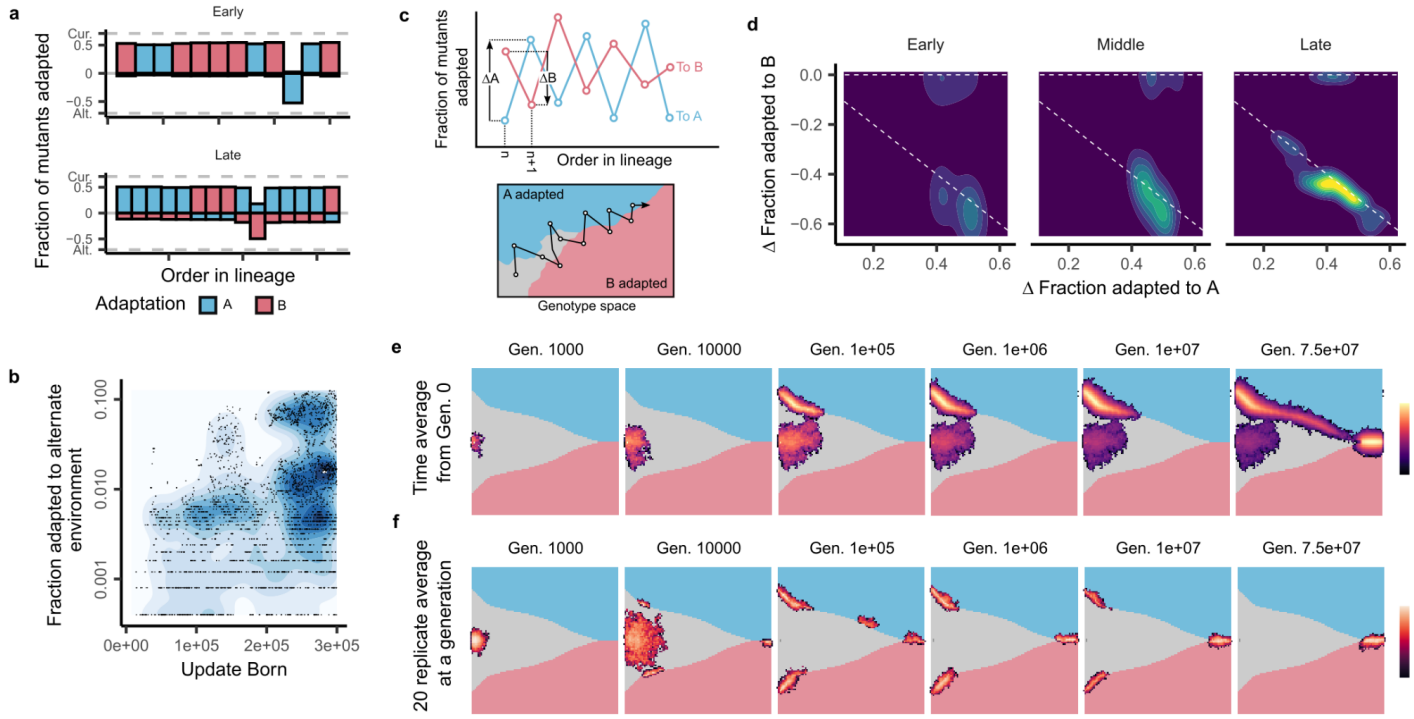

Figure 5: Local mutational landscape of lineages in a changing environment. (**a**) Fraction of single point mutants adapted to the current (positive) and the alternate (negative) environment along a lineage under the *Cyclic* regime early and late in evolution. The y-axis has been square root scaled for clarity. The x-axis denotes the index of the mutational event in the dominant lineage when a new genotype appeared (counting from the ancestral genotype). The color of the positive bar denotes the environment state when the genotype appears in the lineage. Only two representative time intervals from a single replicate are plotted here. Early and late curves are from updates 10,000-15,000 and 295,000-300,000 respectively. (**b**) Fraction of point mutants adapted to the alternate environment as a function of the update that the genotype appeared in the lineage. Mutation events from all replicates under the *Cyclic* regime are plotted together (n=10). Lineage genotypes that failed to track the environment have been removed for clarity. The background density plot depicts a kernel density estimate of the entire data. (**c**) Schematic for calculating mutational tradeoffs along the lineage. ΔA and ΔB are calculated as the change in the fraction of single mutants that are adapted to environment A and B, respectively, between genotype n and $n+1$ on the lineage (top). A hypothesized model of evolvability that would imply increasing mutational tradeoffs along the lineage (bottom). (**d**) Density plot for points denoting ΔB and ΔA at steps on the dominant lineage from early, middle, and late evolution. ΔA values less than 0.1 have been excluded for clarity (See Extended Data Figure 5 for the complete data). The sloped white line denotes a 1:1 tradeoff between the number of mutants adapted to the different environments when a mutation appears in the lineage. (**e**) Simulation of a Wright-Fisher population evolving on a 2D genotype-phenotype map. Background color denotes the phenotype and foreground heatmap denotes the time-average population density in the genotype space from the start of the simulation until the labeled generation number (single replicate, log-scaled). (**f**) Average population density on the genotype space for an ensemble of replicate populations at different times during evolution (n=20, log-scaled).

METHODS

Avida simulations and setup

We used the Avida Digital Evolution Platform to perform evolution experiments[30]. In Avida, organisms are autonomous, asexual, self-replicating computer programs that compete for space and processing time in a virtual environment. Organisms possess a genome - a linear sequence of computer instructions - that enables them to reproduce and perform computational functions. The set of instructions includes operations for basic computations, flow control (e.g., conditional logic and looping), input, output, and the building blocks of self-replication. To reproduce, organisms must copy their genome instruction-by-instruction and then divide. Copy operations are imperfect and result in single-instruction mutations in the offspring's genome. Time in Avida is measured in updates. An update occurs after 30 instructions in an organism's genome have been executed, on average. The average generation time of an Avida organism in these experiments is around 10 updates. All experiments were performed for 300,000 updates (around 30,000 generations). A complete list of parameter values used in these simulations is given in Supplementary Information Table 1.

For experiments conducted in this work, we limited the carrying capacity of the Avida world to 22,500 organisms. On division, new offspring are placed randomly in the world, replacing any existing occupants. Organisms thus compete for space, which also drives selection to improve their replication rate in order to not be overwritten by competitors. Performing computations allow the organisms to acquire a fitness multiplier depending on the environment. We used two environments - A and B - that rewarded an alternate set of computations or tasks. *Environment A* rewarded the organisms with a fitness multiplier of 2.0 if they performed tasks NOT, AND, or OR - and penalized NAND, ORN, or ANDN with a multiplier of 0.8. *Environment B* rewarded the organisms with a fitness multiplier of 2.0 for NAND, ORN, or ANDN - and penalized NOT, AND, or OR with a 0.8 multiplier. The rewards and penalties stacked, thus providing the maximum fitness benefits to organisms that were perfectly adapted to perform only the tasks rewarded in each environment.

We initiated all evolution experiments with identical ancestral organisms having a 100-instruction genome. Organism genome lengths were fixed at this size. For all the experiments, we used a copy mutation rate of 0.001, which created approximately one substitution out of every 1000 instructions copied. For most of the analyses described below, the genotype with the highest frequency in the population at the end of the experiment - the dominant genotype - was used as the representative genotype from the evolved population.

Environment change regimes

The environment change regime determines the way environments switch in an experiment. The *Const-A* and *Const-B* regimes were in environment states *A* and *B*, respectively, throughout evolutionary time. The *Cyclic* regime switched between environments *A* and *B*, with the waiting time between switches picked from a Gaussian distribution with a mean of 300 updates and a standard deviation of 60 updates. The *Cyclic (Fast)* regime switched between *A* and *B* with a mean waiting time of 30 updates and a standard deviation of 6 updates. The *Cyclic (Slow)* regime switched between *A* and *B* with a mean waiting time of 3000 updates and a standard deviation of 600 updates. In the *Random* regime, tasks to be rewarded or penalized were picked randomly from the set of six tasks described before. All regimes ended with 300 updates of evolution in a constant terminal environment (environment *A* for all regimes except *const-B*). Evolution in these terminal environments allowed us to compare adaptive states at the end of the experiments consistently across regimes.

Analysis of mutational landscape

We performed an exhaustive survey of the mutational neighborhood of the dominant genotype from the end of the experiments. To do so, we created every possible single and double point mutation in the dominant genotypes isolated after evolution. We tested each mutant for viability (i.e., the ability to self-replicate) and measured its phenotype (i.e., the set of tasks the mutant could perform). For mutational landscape analysis of genotypes along a lineage (rather than the final dominant genotypes), only single point mutations were created. The data from single and double point mutation landscapes was found to be largely consistent across treatments (Figure 3b).

Pointwise mutual information

The pointwise mutual information (PMI) for two events $x, y \in \Omega$ is defined as,

$$pmi(x,y) = log_2\left(\frac{P(x,y)}{p(x)p(y)}\right)$$

Where Ω is the sample space of events, p is the probability mass function on Ω, and P is the probability mass function on the joint sample space $\Omega \times \Omega$. We normalized this value between -1 and 1 by defining the normalized pointwise mutual information as

$$npmi(x,y) = \frac{log_2\left(\frac{P(x,y)}{p(x)p(y)}\right)}{-log_2(P(x,y))}$$

The NPMI measures the excess probability of occurrence for certain event pairs in the joint probability distribution when compared to the expected distribution based on these events' marginal probabilities.

For the measurements in this work, x and y denote the different tasks in the set of possible tasks recognized by the environments. $p(i)$ was measured as the fraction of all possible single and double mutants that performed the task i. $P(i,j)$ was measured as the fraction of all possible single and double mutants that performed both tasks i and j. A positive NPMI denotes that the task pair was overrepresented in the double mutation neighborhood than expected from the marginal probabilities of its components. A negative NPMI denotes that the task pair was underrepresented on average.

The sample space $S = \Omega \times \Omega$ consists of 36 possible task pairs. Task pairs were labeled as cognate ($\in S_c$) or non-cognate ($\in S_N$) depending on whether they were rewarded by the same environment or not, respectively. The total NPMI was calculated as the sum of individual NPMIs after assigning the task pair a sign based on its cognate/non-cognate label, i.e.,

$$\text{Total } npmi = \sum_{(x,y)\in\Omega\times\Omega} s * npmi(x,y)$$

Where,

$$s = 1, \text{ if } (x,y) \in S_c$$
$$= -1, \text{ if } (x,y) \in S_N$$

We used this total NPMI metric to compare information encoded on the mutational landscape of the dominant genotypes obtained across treatments.

Likelihood of phenotype change

We surveyed the single-point mutation landscape of genotypes obtained along the lineage and measured the phenotypes for these mutants. Using this data, we calculated the likelihood of a realized phenotype as its fractional abundance in the single mutational neighborhood of the previous genotype in the lineage. The rarity of the phenotype was then calculated by taking a negative log (base 10) of this fraction. For example, a rarity of 3 denotes that the realized phenotype along the lineage was expressed in only 1 out of 10^3 point mutants of the previous genotype in the lineage.

METHODS

Tradeoffs along the lineage

Tradeoffs along the lineage were measured by calculating the change in the fraction of mutants adapted to environment A (ΔA) and environment B (ΔB) between mutants occurring along the lineage (Figure 5d, Top). Points with coordinates (ΔA,ΔB) were then plotted in a 2D Cartesian plane (Extended Data Figure 5). For Figure 5c, we calculated the density of these points in the fourth quadrant using a kernel density estimate. Points along the axes of the 2D plane indicate mutation events along the lineage where an increase or decrease in mutants with one adaptation was not accompanied by a change in the number of mutants with the other adaptation. A high density of points along the $y = x$ line denotes a concordant increase in mutants adapted to both environments. A high density of points along the $y =- x$ line denotes a 1-to-1 tradeoff, where an increase in mutants adapted to one environment comes at a cost to the number of mutants adapted to the other.

Evolution on a 2D genotype space

To perform simulations of evolution on a structured genotype space, we created a program to run Wright-Fisher dynamics with custom phenotypic mappings. More documentation for this program is available at the link specified in the software availability statement. This framework simplifies the visualization of evolutionary dynamics in a genotype space by abstracting it to 2-dimensions. A genotype in this simulation is a tuple of integers with four possible point mutants, one along each of the four cardinal directions. Population size is assumed to be constant throughout evolution and was fixed at 10,000 organisms for all 20 replicates in this study. A complete list of parameters used for these simulations is available in Supplementary Information Table 2.

Mutations are made by sampling an integer (k) from a poisson distribution with a rate parameter $\ln(1/(1-\mu))$ for each sampled genotype, where μ is the mutation probability. Then, k mutations are made to the genotype by randomly choosing one of the four directions to mutate in. Thus, the probability of a Wright-Fisher sampled genotype acquiring no mutations in a generation is $(1-\mu)$. The mutation probability was fixed at $\mu = 10^{-2}$ for all simulations presented here. The genotype-phenotype map was fixed at the one shown in Extended Data Figure 6a. The blue region in this figure denotes genotypes adapted to environment A. The red region denotes genotypes adapted to environment B. The grey region denotes genotypes that had an intermediate phenotype between the two adaptations. For the simulations in Figure 5, the environment switched between the two environment states with a Poisson rate parameter $p_{switch} = 0.01$, thus switching every 100 generations on average. In environment A, the A-adapted genotypes had a relative fitness of 2.0 and the B-adapted genotypes had a relative fitness of 0.8, compared to the intermediate phenotype. In environment B, the B-adapted genotypes had a relative fitness of 2.0 and the A-adapted genotypes had a relative fitness of 0.8. All simulations were run for 75 million generations. The initial population was initialized as a clonal population with all 10,000 genotypes in the population belonging to the region to the far left of the intermediate phenotype region (dark-grey squares in Extended Data Figure 6a).

Software availability

Avida, the open-source digital evolution framework used in this work, is available under the MIT license at https://github.com/devosoft/avida. The build files for the simgpm.rs program used to simulate wright-fisher populations on a custom genotype space are available under the MIT license at https://github.com/kumawatb/simgpm_rs (archived at https://doi.org/10.5281/zenodo.7487450). This program was written in the Rust programming language[51]. We used Python for data processing and R for data wrangling and visualizations[52,53]. In addition, the following R packages were used: *ggplot2, tidyverse, cowplot, viridis, RColorBrewer, scales, svglite, latex2exp, reshape2, scico,* and *ggpubr*[54–64].

Data availability

All data used in this work has been archived publicly at https://www.dropbox.com/sh/gwxpo5ox76c7np7/AAB6fIqc4NlGyT01TzOp5Bpta, along with the scripts and analysis files. These include the configuration files used for Avida and the Wright-Fisher simulations.

Acknowledgments

We thank Dr. Jordan Horowitz for his valuable comments. This research was supported in part through computational resources and services provided by Advanced Research Computing at the University of Michigan, Ann Arbor, and Funding from the NSF (DEB 1813069).

Author contributions

BK and LZ wrote the manuscript, BK, AL, MA, and LZ conceived of the project, designed the experiments, and ran the analyses. BK developed the Wright-Fisher simulations. All authors edited and reviewed the manuscript. LZ supervised and funded the work.

Competing Interests

The authors declare no competing interests.

Materials & Correspondence

Correspondence and materials requests should be addressed to Luis Zaman (zamanlh@umich.edu).

Methods References

51. Matsakis, N. D. & Klock II, F. S. The rust language. in *ACM SIGAda ada letters* vol. 34 103–104 (2014).
52. Van Rossum, G. & Drake, F. L. *Python 3 reference manual*. (CreateSpace, 2009).
53. R Core Team. *R: A language and environment for statistical computing*. https://www.R-project.org/ (2022).
54. Wickham, H. *ggplot2: Elegant graphics for data analysis*. (Springer-Verlag New York, 2016).
55. Wickham, H. *et al.* Welcome to the tidyverse. *J. Open Source Softw.* **4**, 1686 (2019).
56. Wilke, C. O. *cowplot: Streamlined plot theme and plot annotations for 'ggplot2'*. https://CRAN.R-project.org/package=cowplot (2020).
57. Garnier *et al. viridis - colorblind-friendly color maps for R*. https://sjmgarnier.github.io/viridis/ (2021) doi:10.5281/zenodo.4679424.
58. Neuwirth, E. *RColorBrewer: ColorBrewer palettes*. https://CRAN.R-project.org/package=RColorBrewer (2022).
59. Wickham, H. & Seidel, D. *scales: Scale functions for visualization*. https://CRAN.R-project.org/package=scales (2022).
60. Wickham, H. *et al. svglite: An 'SVG' graphics device*. https://CRAN.R-project.org/package=svglite (2022).
61. Meschiari, S. *latex2exp: Use LaTeX expressions in plots*. https://CRAN.R-project.org/package=latex2exp (2022).
62. Wickham, H. Reshaping data with the reshape package. *J. Stat. Softw.* **21**, 1–20 (2007).
63. Pedersen, T. L. & Crameri, F. *scico: Colour palettes based on the scientific colour-maps*. https://CRAN.R-project.org/package=scico (2022).
64. Kassambara, A. *ggpubr: 'ggplot2' based publication ready plots*. https://CRAN.R-project.org/package=ggpubr (2022).

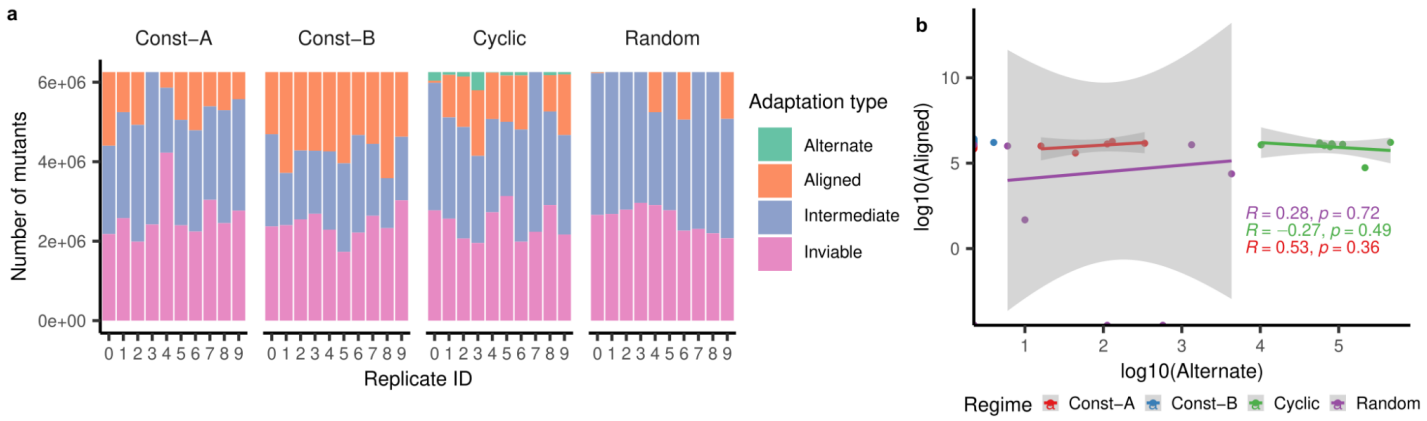

Extended Data Fig 1. Distribution of mutant adaptations after evolution. (**a**) The number of mutants of the dominant genotype - isolated from populations evolved in the four regimes - that are either perfectly adapted to the terminal environment (orange), the environment alternate to the terminal (green), have an intermediate phenotype (blue), or are inviable (unable to self-replicate, pink). Each bar corresponds to one dominant genotype from a replicate population evolved under a particular environment change regime. Adaptations for both single $(n = 2500)$ and double mutants $(n = 625000)$ have been plotted here. Note that the y-axis is not log scaled, unlike Figure 2 in the main text. (**b**) A plot of the number of alternate mutants plotted against the number of mutants aligned to the terminal environment (log-scaled). The color of the points denotes the regime and each point stands for the dominant genotype from a replicate population. The lines denote a linear regression with the grey regions highlighting the 95% confidence intervals. Pearson's correlation coefficient (R, two-sided) and p-values are given for three of the four regimes.

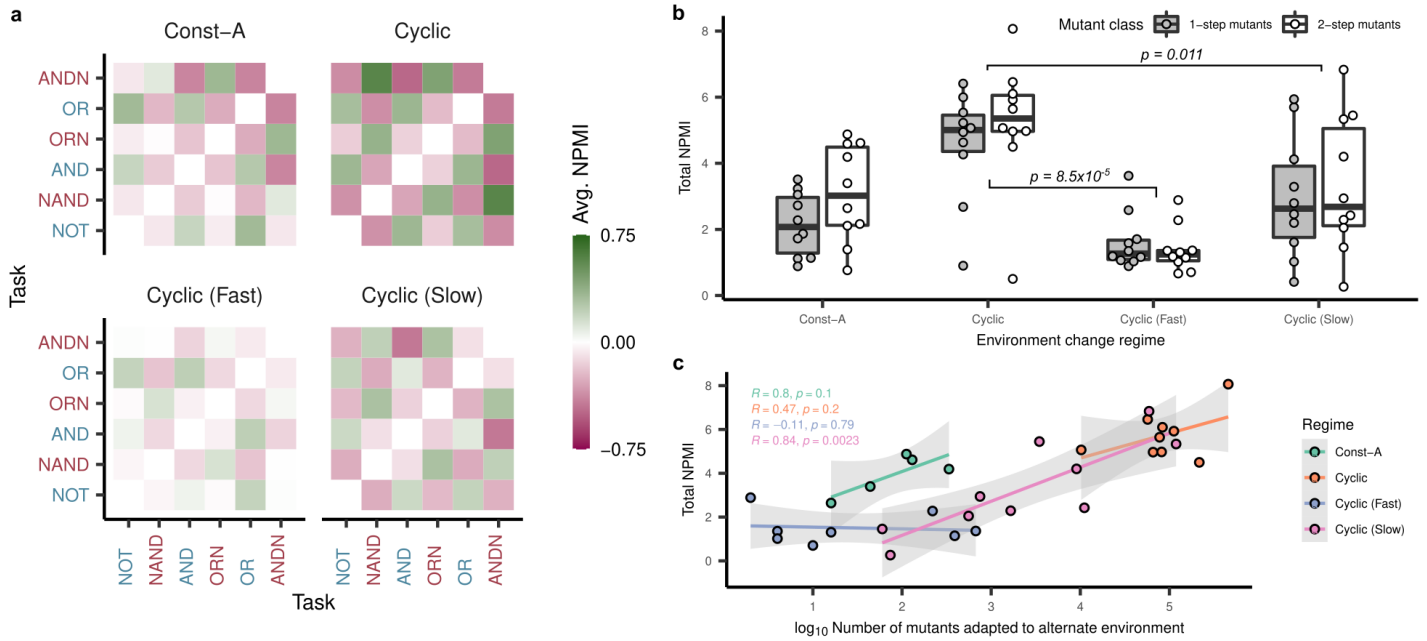

Extended Data Fig 2. Information in the mutation landscape at extreme environment change rates. (**a**) Heat maps denote the normalized pointwise mutual information (NPMI) values between different task pairs for dominant genotypes isolated from populations evolved in *Const-A* and three *Cyclic* regimes with different mean waiting times ($\mu_{Cyclic\ (Fast)} = 30$, $\mu_{Cyclic\ (Slow)} = 3000$). The marginal and joint probabilities for different tasks are calculated using only the double mutants of the dominant genotype at the end of the simulation. Labels in blue and red denote tasks rewarded in environments A and B, respectively. Tasks rewarded together in an environment are defined as *cognates*. The NPMI values for each task pair have been averaged across the 10 replicates. (**b**) Total NPMI for task pairs for Const-A, and the three different cyclic regimes. The total NPMI was calculated by adding up individual NPMI values after assigning them a sign based on the cognate/non-cognate nature of a task pair (n=10). Each point denotes the total NPMI calculated using the single or double mutants of the isolated dominant genotypes from 10 different replicate populations. Boxplot characteristics are the same as in Figure 2b. NPMI values were found to be significantly different between regimes but not between mutant classes (two-way ANOVA; regime F = 17.349; regime df = 3; regime p-value = 1.41e-08***; class F = 1.605; class df = 1; class p-value = 0.209). Pairwise p-values shown in the figure are calculated using a two-tailed Wilcoxon rank-sum test (p-values adjusted using the Benjamini-Hochberg method). (**c**) Total NPMI as a function of the number of mutants adapted to an environment alternate to the terminal for the four regimes. Each point is the NPMI and mutant adaptations calculated from the dominant genotype from a replicate. The x-axis is log-scaled and any data points with zero mutants adapted to the alternate environment have been removed. The lines denote a linear regression with the grey regions highlighting the 95% confidence intervals. Pearson's correlation coefficient (R, two-sided) and p-values are given for the four regimes.

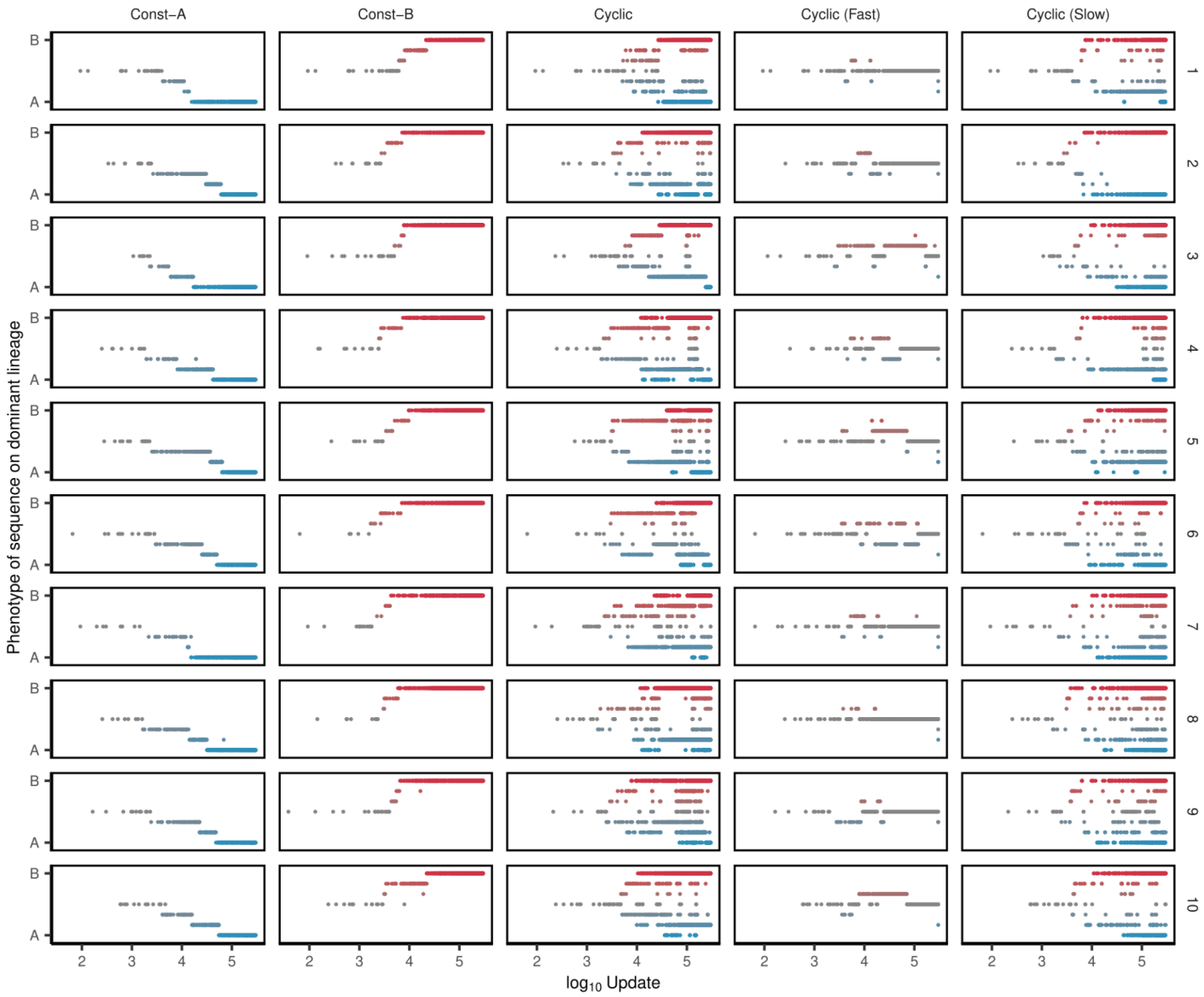

Extended Data Fig 3. Lineages in a constant environment reach phenotypic stasis. Task configuration of sequences along the dominant genotype lineage over evolutionary time. Task configuration is calculated as the minimum number of task losses/gains required to be perfectly adapted to environment A, or the Hamming distance of the phenotype from a phenotype perfectly adapted to environment A. Genotypes on the A and B lines on this graph are perfectly adapted to the respective environments. Columns denote the different environment change regimes and rows are individual replicates. Each point is a single mutation event along the lineage. Note that the x-axis is log-scaled.

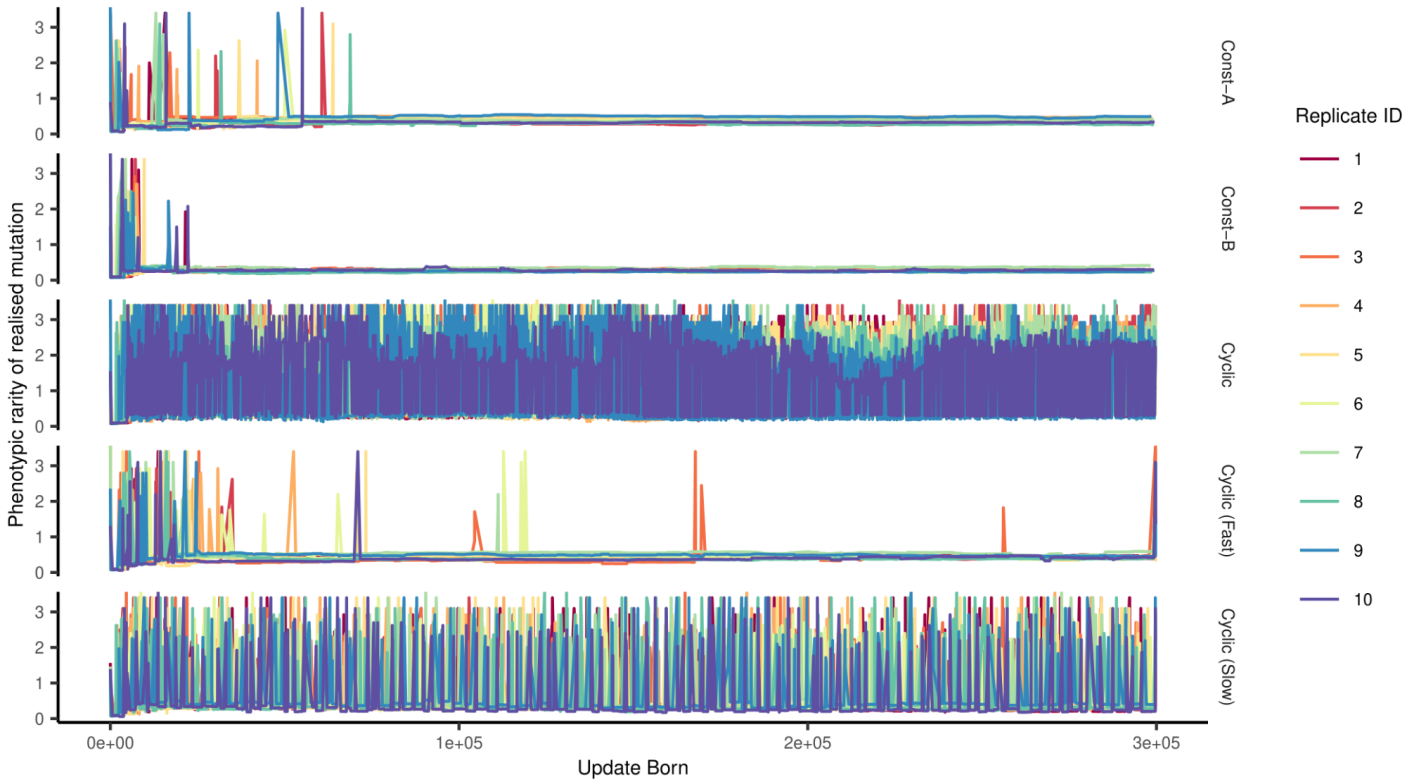

Extended Data Fig 4. Environment fluctuation rate affects signatures of adaptation along the lineage. The rarity of phenotypic mutations along the lineage during evolution in *Const-A*, and three *Cyclic* regimes with different mean waiting times. Rarity is measured as the negative log-likelihood of a phenotype change that appears in the lineage, on the single mutation landscape of the previous sequence in the lineage. Each curve is a dominant genotype lineage from different replicate populations (n=10).

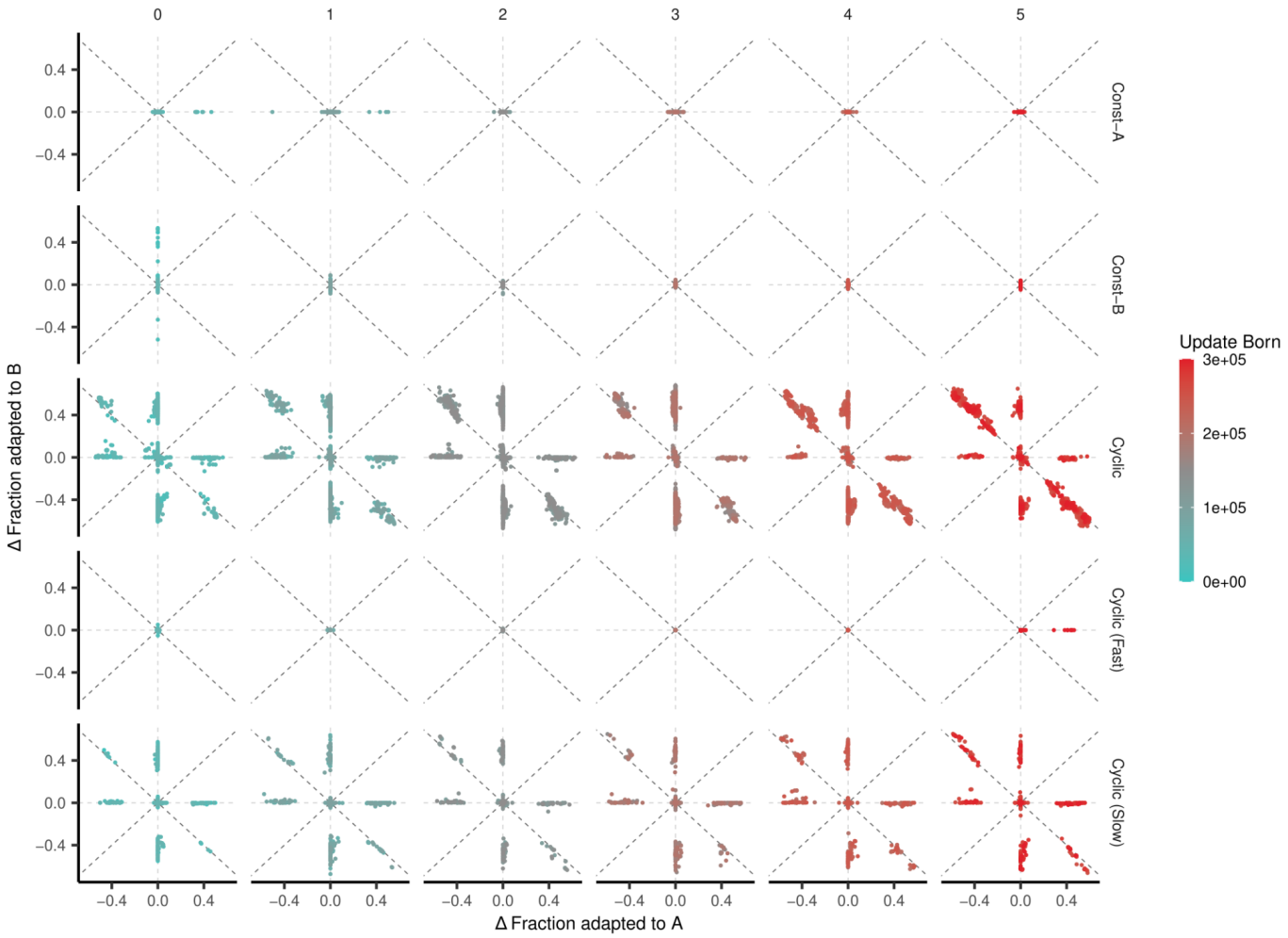

Extended Data Fig 5. Mutational tradeoffs in different regimes. Points denoting ΔB and ΔA (see Figure 5) at steps on the dominant lineage from six time intervals during evolution (equally spaced, each spanning 50,000 updates). Points from all replicates in each of the regimes are plotted here (n=10). The color of the points denotes the update at which the particular mutation event is seen in the lineage. Points on the dark-grey lines denote a 1:1 tradeoff ($y = -x$) or a correlation ($y = x$) between the number of mutants adapted to the different environments when a mutation event appears in the dominant genotype lineage. Points on the light-grey lines ($y = 0$) denote no tradeoff, i.e., when mutation events on the lineage lead to an increase or decrease in mutants adapted to one of the environments with no change in mutants adapted to the other environment. Note that no positive correlations are observed between the two fractions (no points in the first or third quadrants), indicating that a gain in mutants adapted to an environment is either always accompanied by a loss in the number of mutants adapted to the alternate environment, or has no effect on this number.

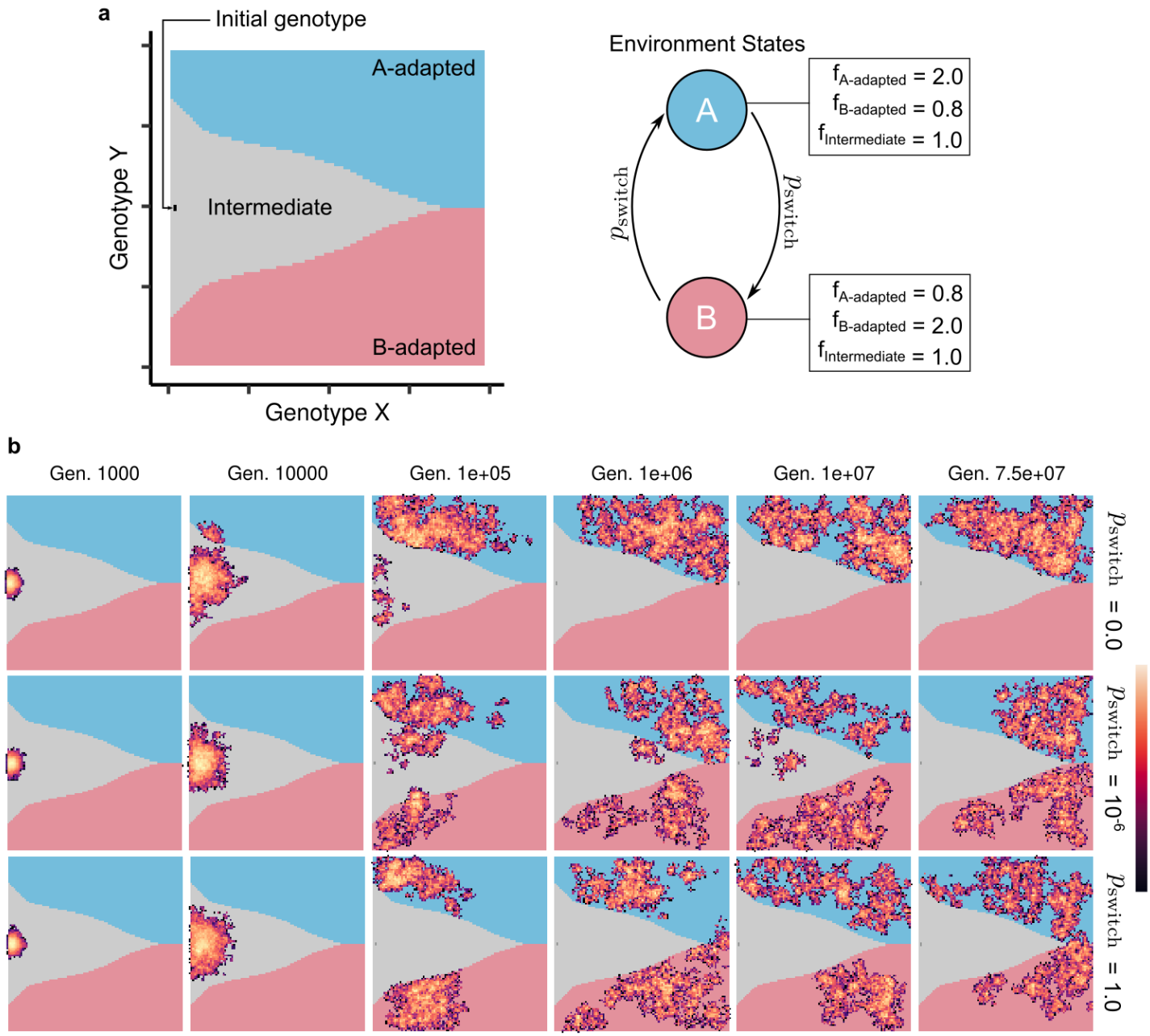

Extended Data Fig 6. Schematic of 2D genotype space experiments and localization in constant and fluctuating environments. (**a**) 2D genotype-phenotype map used to simulate evolving populations (left). The genotype space has 100x100 genotypes with each pixel denoting a single genotype. The color of the pixel denotes the phenotype and each genotype has its four cardinal neighbors as single mutants. The environment switches between two states, A and B, with a Poisson rate parameter p_{switch} (right). A-adapted and B-adapted genotypes have different fitness values in the two environments, as indicated in the boxes. (**b**) Average population density on the genotype space for an ensemble of replicate populations at different times during evolution (log-scaled, n=20). The $p_{switch,,}$ values are varied between 0.0 (no switching), 10^{-6} (average switching time of 1 million generations), and 1.0 (environment switches every generation). Population density has been log-scaled for clarity.